A Micromachined Finite Coplanar Line-to-Silicon Micromachined Waveguide Transition For Millimeter and Submillimeter Wave Applications

Yongshik Lee, James P. Becker*, Jack R. East, Linda P. B. Katehi

Radiation Lab and Solid State Electronics Lab, University of Michigan, Ann Arbor, Michigan,
*Electrical and Computer Engineering, Montana State University, Bozeman, Montana

Abstract — **A finite ground coplanar (FGC) line-to-waveguide transition utilizing a novel, free-standing printed E-plane probe has been demonstrated in *W*-band (75-110GHz). One way to improve the performance of such a transition and to extend its utility well into the submillimeter range is to thin the supporting substrate beneath the probe. This paper presents the *W*-band performance of a fully micromachined finite ground coplanar line-to-silicon diamond waveguide transition with the substrate beneath the probe entirely removed, thus forming a free-stranding metal structure.**

I. INTRODUCTION

FGC line has become one of the most widely used transmission lines in millimeter and submillimeter applications. However, rectangular waveguides still play an important role for high frequency sources, THz range for example. Thus, a transition between the two types of transmission lines can be critical in many applications. The FGC line-to-waveguide transition presented previously in [1] and [2] by the authors is depicted in Fig. 1, in a back – to-back configuration. A rectangular metal probe is inserted into a waveguide through its broadside wall. The probe is fed by extending the center conductor of the FGC line. The size of the probe, its relative position with regards to the waveguide sidewalls, and the distance between the probe and the waveguide backshort are the key factors affecting transition performances in terms of bandwidth, return loss, and insertion loss.

Another critical factor that affects the transition performance is the amount of stored energy in the probe structure. It is well known from the electromagnetic theory that the effective permittivity of a probe can be reduced if the substrate under the probe is thinned, or if we use substrate material with a lower permittivity. Lower effective permittivity in turn means less energy stored in the substrate, and results in improved transition performance. Below we demonstrate a means to minimize the stored energy immediately beneath the probe through complete removal of the supporting silicon substrate. Such a structure is demonstrated to maintain its mechanical integrity.

II. MOTIVE

In the previous work by the authors, a finite ground coplanar line-to-conventionally machined rectangular waveguide transition operating in *Ka*-band and a finite ground coplanar line-to-silicon micromachined diamond waveguide transition operating in *W*-band were presented. The transition utilized a rectangular probe printed on a silicon wafer. Compared with previous works reported in the literature [3]-[4], improved insertion losses and wider 10dB return loss bandwidths were demonstrated [1]-[2].

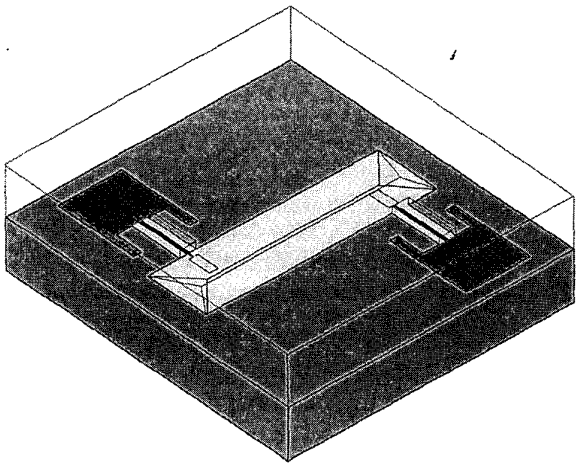

Fig. 1. Schematic diagram of fully micromachined FGC line-to-silicon diamond waveguide transition module. The top half is drawn as transparent.

A major difficulty in this transition is the required thinning of silicon wafer in order to achieve good

0-7803-7239-5/02/$10.00 © 2002 IEEE

performance. In the previous work, the *Ka*-band probe was fabricated on a 500μm-thick silicon wafer and the silicon substrate under the probe was etched to half of the original thickness in order to improve the performance of the transition. As the *Ka*-band design was scaled down for operation in *W*-band, the substrate under the probe had to be etched down to less than 100μm, to provide a comparable level of performance. The thinned silicon substrates were difficult to fabricate from thicker wafers. In order to overcome this problem, the earlier *W*-band probes were fabricated on a 100μm, which made it unnecessary to thin down any part of the wafer.

If the substrate supporting the probe is made even thinner as required at higher frequencies, it is expected that the transition performance will improve due to a reduction in the stored energy in the substrate. As we go higher in frequency, the substrate thickness under the probe has to be thinner in order to retain the same-scaled dimension. Also, as the operating frequency is increased, the substrate thickness under the probe must be thinner for the probe structure to properly fit within the waveguide whose dimensions must likewise shrink in accordance with the increased operating frequency. Eventually, complete removal of the substrate beneath the probe may in fact become necessary.

When the substrate under the probe is completely removed, the probe may have better mechanical strength than when it is etched locally and partially since the remaining substrate is of a single thickness. In this case, the metal probe has to have certain mechanical strength in order to be suspended in air. In addition, control of the stress in the metal layers comprising the probe becomes crucial in preventing the suspended probe from warping.

III. Fabrication

For measurement purposes, a back-to-back structure of this transition was fabricated as in [1]. The input and output are both FGC lines, and in between the two probes, there is a 0.83cm section of a diamond waveguide. This is depicted in Fig. 1. Compared with the original *W*-band design, the probe is approximately 1.05 times larger in size, 608μm×202μm, but the ratio of width to length of the probe has been kept the same. In order to account for the reduced electrical length of the probe due to a smaller effective permittivity, the size of the probe has to be larger. However, increasing the probe size increases the possibility that the air-suspended probes will bend down because of weight, or curl up due to stress. The major dimensions of the transitions presented in this work and of the original work[1] are summarized in Table 1.

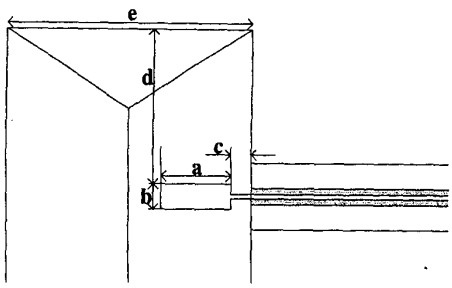

Fig. 2. Bottom half of FGC line-to-silicon diamond waveguide transition module. The dimensions are given in Table 1.

TABLE I
SUMMARY OF IMPORTANT DIMENSIONS[μm]

	a	b	c	d[mm]	e
This work	608	202	170	2.0	1796
[1]	579	192	160	1.5	1796

A. Micromachined Probes

The probes are fabricated on a (001)-oriented high resistivity (ρ>2000Ω·cm) silicon wafer with a thickness of 100μm. Arm-like appendages were developed to ensure secure placement of the probes on the bottom half of the waveguide. The first step is to etch through the alignment marks in the deep reactive ion etching (DRIE) system. These etched-through vernier and cross alignment marks are used for backside alignment.

Due to compatibility issues with the fabrication processes of other researchers in our shared facility, gold was not allowed to be used in the deep reactive ion system. In addition, stresses in the metal layers of the metal pattern are a critical issue in fabricating these air-suspended probes. Conductivities for gold and nickel are 4.098×10^7 S/m and 1.449×10^7S/m, respectively, at 20°C [4]. From an electrical loss standpoint gold is clearly preferred. To minimize the possibility of the mechanical deflection of the suspended probe, a relatively thick metallization is desired and realized through metal plating. Due to the degree of inherent stress, plated gold may in fact be more difficult to utilize in our structure than nickel. Further investigation is needed to access the potential of utilizing gold in the reported transition structure.

2000Å of titanium and 500Å of nickel are evaporated as the seed layer. Photolithography is done using the etched-through alignment marks and approximately 8μm of nickel

is plated at a plating rate of about 0.13μm/min. The remaining photoresist is then stripped and the seed layer is removed. Then the wafer is flipped over for backside processing. Photoresist with thickness of approximately 8μm is spun over the wafer. Again, photolithography is done using the etched-through alignment marks. The substrate under the probe is etched by DRIE and at the same time, the probes are released from the wafer. Then the 2000Å titanium layer of the probe, now exposed after complete removal of the silicon substrate under the probe, is etched in hydrofluoric acid:deionized water (1:10). This was done to relieve the stress coming from the interface between the titanium and the nickel. Finally, the photoresist is stripped and the probes are cleaned in acetone and isopropyl alcohol (IPA).

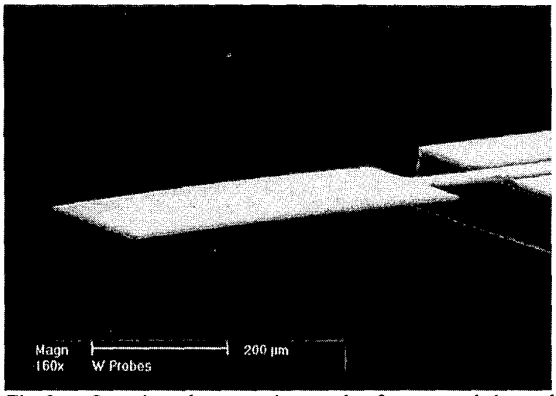

Fig. 3. Scanning electron micrograph of a suspended metal probe formed by deep reactive ion etching of the underlying silicon substrate.

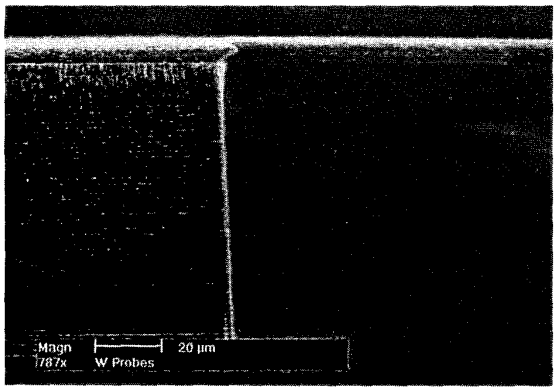

Fig. 4. Cross sectional view of the suspended probe. The silicon wafer is 100μm thick.

A scanning electron micrograph of a fabricated probe is shown in Fig. 3. As can be seen, about 8μm of nickel is thick enough to provide mechanical strength to the probe to keep it suspended in air. Also, the warping effect of the probe due to stress is negligible. A cross sectional view of the edge of the probe is given in Fig. 4. The deep etching recipe utilized (see [2] for details) results in a nearly vertical sidewall as evidenced by the figure.

B. Silicon Micromachined Diamond Waveguide

The silicon micromachined diamond waveguide is fabricated in a similar manner as in [1]. A (001)-oriented high resistivity (ρ>1000kΩ·cm) silicon wafer with a thickness of 2mm has been etched in 25% tetramethyl ammonium hydroxide (TMAH) to form top and bottom halves of a diamond waveguide. The etch depth is 1270μm, which is one half of the *W*-band standard waveguide (WR-10) height. At the same time, pits for glass microspheres for aligning the two halves of a waveguide are etched.

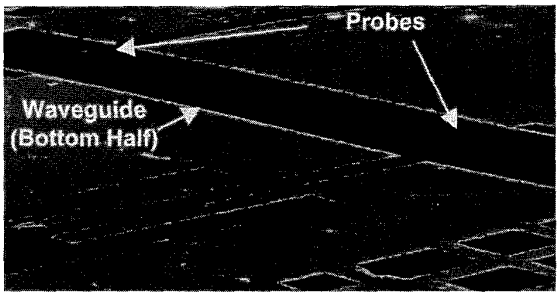

Fig. 5. Scanning electron micrograph of a bottom half of silicon diamond waveguide with probes placed in the cradle. Pits for aligning the top and bottom waveguide pieces are shown in lower-right corner.

The next step is to etch necessary grooves by deep reactive ion etching (DRIE). Grooves in the bottom half of a waveguide serve as the cradle for the fabricated probes, and grooves in the top half of a waveguide serve as the shields over the FGC lines. Before applying photoresist, 5000Å of titanium is sputtered over the entire wafer. This titanium layer is used as another masking layer, in addition 8μm of photoresist, when etching the grooves. This is especially important for the immediate edges of the waveguide where the resist becomes too thin to mask deep reactive ion etching. Insufficient masking of the waveguide edges may result in etching damage along the waveguide, which in turn may degrade overall transition performance through signal leakage. After standard photolithography, apertures for both grooves are opened. Then the sputtered titanium layer in these apertures is etched in hydrofluoric acid:deionized water (1:10). Small pieces of 100μm thick silicon wafer are used together to monitor etching and to

obtain the desired depth of 100μm. The waveguide halves are then diced and 500Å of titanium and 1.6μm of gold are sputtered to metallize the waveguide walls and the grooves. A scanning electron micrograph of a bottom half of a silicon diamond waveguide with two probes placed in the cradles is in Fig. 5.

IV. Measurements And Results

The fabricated back-to-back transition module was measured using an HP 8510C vector network analyzer and GGB picoprobes of 120μm pitch. Calibration was achieved using thru-reflect-line (TRL) protocol with on-wafer FGC thru, short, and delay lines of the same geometry as that used to feed the probe. From TRL calibration, it was calculated that the nickel-plated FGC line has loss of about 4.4dB/cm at 85GHz and about 4.8dB/cm at 105GHz. As in [1], the loss in the diamond waveguide is predicted using Ansoft HFSS, assuming a finite conductivity ($5\times10^6(\Omega\cdot m)^{-1}$) for the walls. Fig. 6 displays the measured results of a back-to-back transition with the calibrated line and waveguide loss removed. For comparison, HFSS simulation results for a lossless case are plotted in solid lines. As seen from Fig. 6, there is a great agreement between the simulated and measured results.

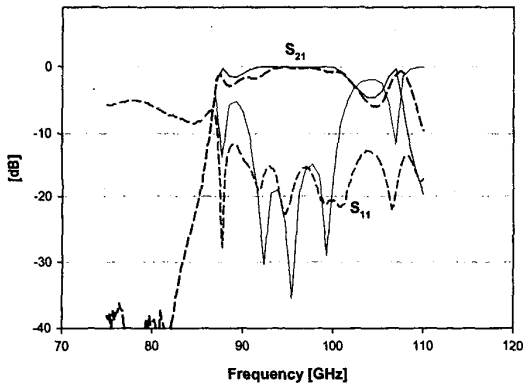

Fig. 6. Measured and simulated results of back-to-back FGC line-to-silicon micromachined diamond waveguide transition. The simulated results are plotted in solid lines.

Measured results show that the waveguide is cutoff below ~87GHz. Above the cutoff frequency, the return loss of the back-to-back transition is better than 10 dB throughout the entire *W*-band, up to 110GHz. The insertion loss is less than 0.5dB per transition from ~92GHz to ~101GHz, and less than 0.25dB per transition from ~93GHz to ~98.5GHz. When compared with the results of [2], the measured S-parameters of Fig. 6 suggest that complete removal of the dielectric may indeed improve the performance of such a planar line-to-waveguide transition. It is certainly expected that when the top and the bottom waveguide halves are thermo-compression bonded (the waveguide halves were simply clipped together in this study), the transition performance will be further improved.

V. Conclusion

The performance of a previously studied fully micromachined FGC line-to-silicon diamond waveguide transition module using an E-plane rectangular probe was improved by completely removing the substrate under the probe. The improvement was significant in terms of 10dB return loss and 0.5dB insertion loss bandwidths. In the work reported here, plated nickel formed the probe metallization. Though more lossy than gold, the mechanical properties of nickel may make it the metal of choice for realizing such transition structures. In addition to exhibiting improved performance over an earlier micromachined version [2], the novel suspended probe structure presented here provides a viable means to effect broadband planar line-to-waveguide transitions well into the submillimeter wave range.

Acknowledgement

This work has been funded by DARPA under the Solid State THz Sources grant #N00014-99-1-0915. The authors would like to thank Dimitrios Peroulis for his help in the fabrication.

References

[1] James P. Becker, Yongshik Lee, Jack R. East, and Linda P.B. Katehi, "A finite ground coplanar line-to-silicon micromachined waveguide transition," *IEEE Trans. Microwave Theory and Tech.*, vol. MTT-49, no. 10, pp. 1671-1676, Oct. 2001.

[2] James P. Becker, Yongshik Lee, Jack R. East, and Linda P.B. Katehi, "A fully packaged finite ground coplanar line-to-silicon micromachined waveguide transition," *Proc. IEEE 9th Electrical Performance of Electronic Packaging Topical Meeting*, pp. 273-276, Oct. 2000.

[3] G. E. Ponchak and R. N. Simons, "A new rectangular waveguide to coplanar waveguide transitions," *IEEE MTT-S International Microwave Symposium Digest*, vol. 1, pp. 491-492, 1990.

[4] G. C. Dalman, "New waveguide-to-coplanar waveguide transition for centimeter and millimeter wave applications," *Electronic Letters.*, vol. 26, no. 13, pp. 830-831, Jun. 1990.

[5] David M. Pozar, *Microwave Engineering*, Addison Wesley, 1998